

Electronic Supplementary Information

**High-Performance Wearable Strain Sensors Based on Fragmentized  
Carbonized Melamine Sponge for Human Motion Detection**

*Xiaoliang Fang<sup>a</sup>, Jianpin Tan<sup>a</sup>, Yang Gao<sup>a,\*</sup>, Yongfeng Lu<sup>b</sup>, and Fuzhen Xuan<sup>a,\*</sup>*

<sup>a</sup>School of Mechanical and Power Engineering, East China University of Science and  
Technology, Shanghai 200237 (China)

<sup>b</sup> Department of Electrical and Computer Engineering, University of Nebraska-  
Lincoln, Lincoln, NE 68588-0511 (USA)

\*E-mail: [yanggao@ecust.edu.cn](mailto:yanggao@ecust.edu.cn) (Yang Gao); [fzxuan@ecust.edu.cn](mailto:fzxuan@ecust.edu.cn) (Fuzhen Xuan)

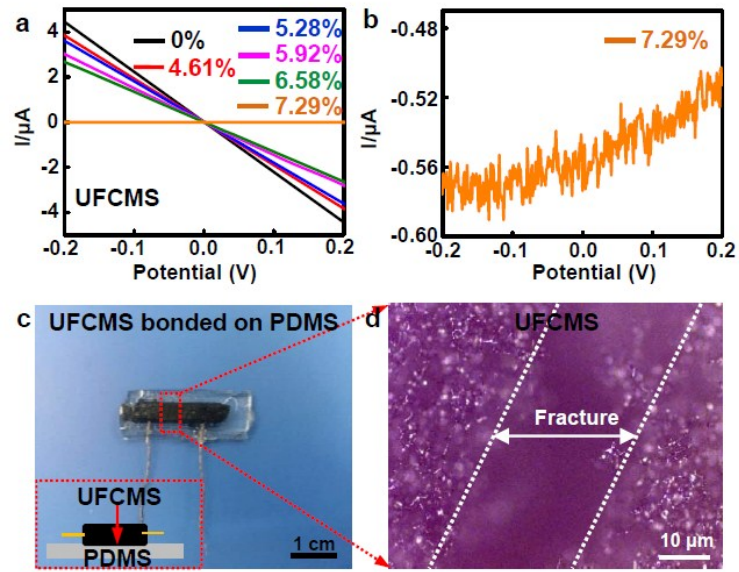


**Figure S1.** (a) and (b) The current-voltage curves of the strain sensors based on UFCMS under various strain loadings. (c) A photograph showing a UFCMS without infiltrated with PDMS for fracture experiment. (d) An optical images of the UFCMS after stretching.

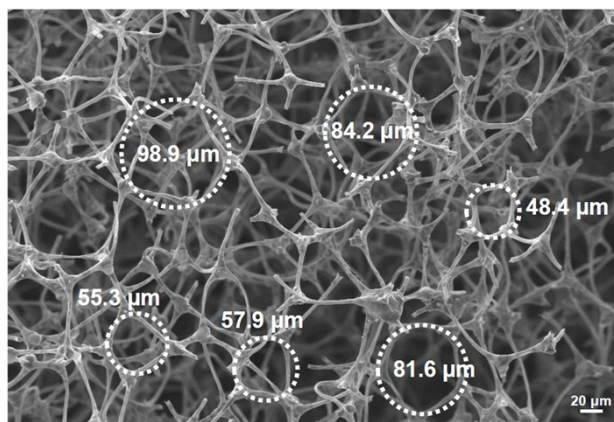
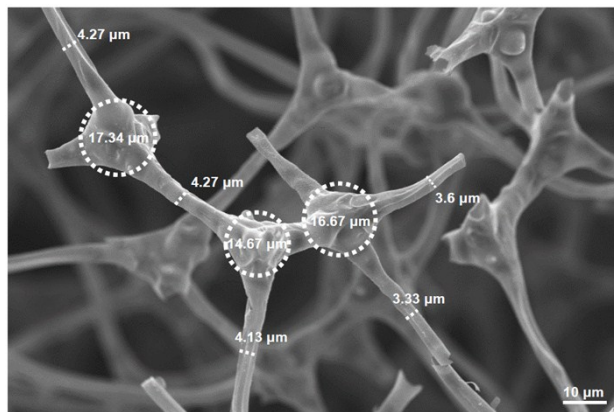


**Figure S2.** SEM images of carbonized melamine sponge.

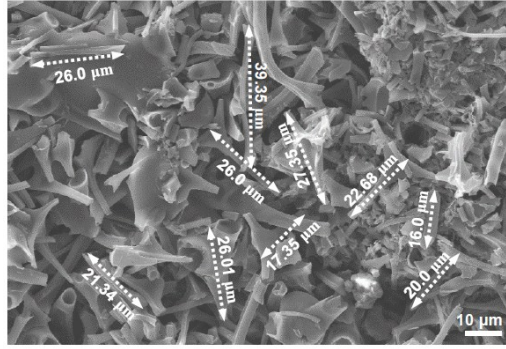


**Figure S3.** SEM image of FCMS powder.

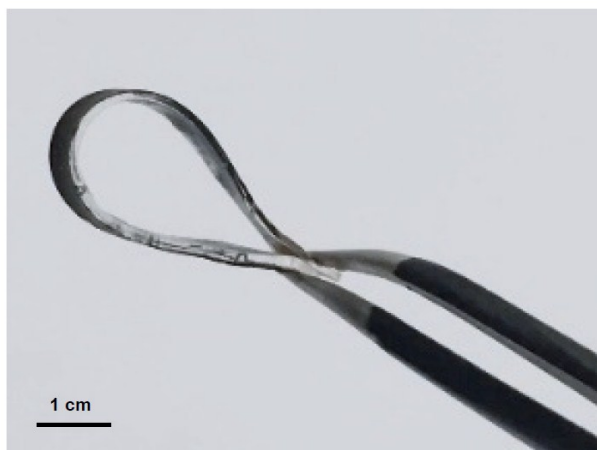


**Figure S4.** A photograph of a FCMS-based strain sensor.

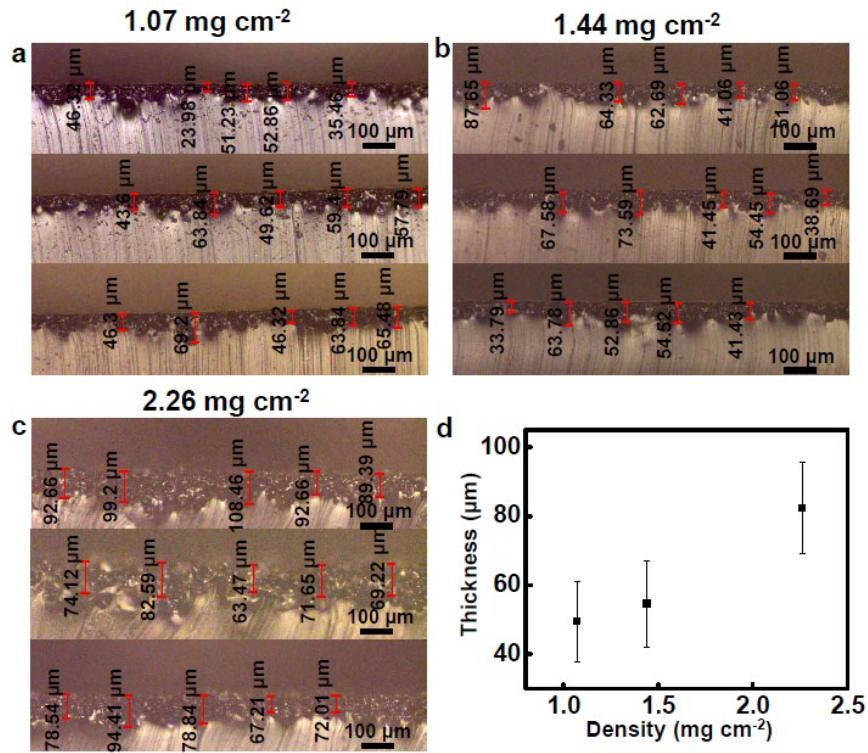


**Figure S5.** (a-c) Optical images of samples with different FCMS densities. (d) The thickness of FCMS-based strain sensors with different FCMS densities.

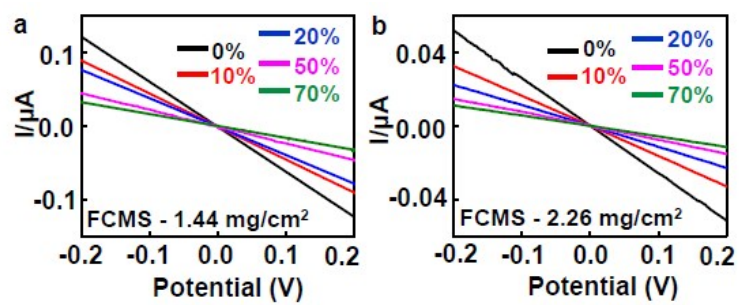


**Figure S6.** Current-voltage curves of the strain sensors with FCMS densities of 1.44 and 2.26  $\text{mg cm}^{-2}$  at different strains.

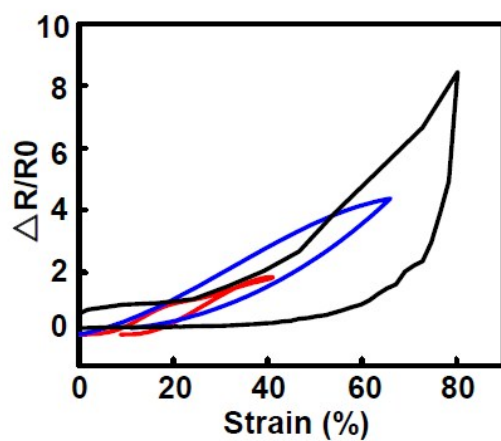


**Figure S7.** Hysteresis curve for the strain sensor with an FCMS density of 1.07 mg  $\text{cm}^{-2}$ .

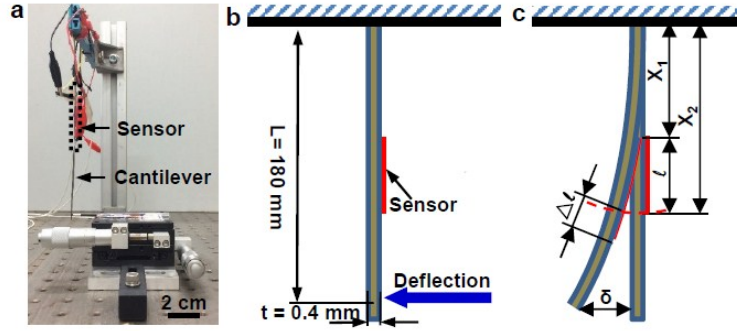


**Figure S8.** The experimental setup for measuring the detection limit of the FCMS-based strain sensor.

**NOTE:** In this study, the cantilever method was used to measure the smallest strain, as shown in Figure S8. The average strain ( $x$ ) at any point of the cantilever can be calculated by the following equation (*Sensor Mater.*, **2014**, 9, 699-709):

$$\varepsilon = \frac{3\delta xt}{2L^3} \quad (1)$$

where  $\delta$  is the applied deflection,  $t$  and  $L$  are the thickness and length of the cantilever, respectively.

The average strain of the FCMS-based sensor can be calculated using the following equations:

$$\varepsilon_{sensor} = \frac{\Delta l}{l} = \frac{\int_{x_1}^{x_2} \frac{3\delta xt}{2L^3} dx}{l} = \frac{\frac{3\delta t}{4L^3} (x_2^2 - x_1^2)}{l} = \frac{3\delta t}{4L^3} (x_2 + x_1) \quad (2)$$

where  $x_1$  and  $x_2$  are the coordinates of the ends of the strain sensor,  $l$  is the length of the sensor, which equals to  $x_2 - x_1$ .

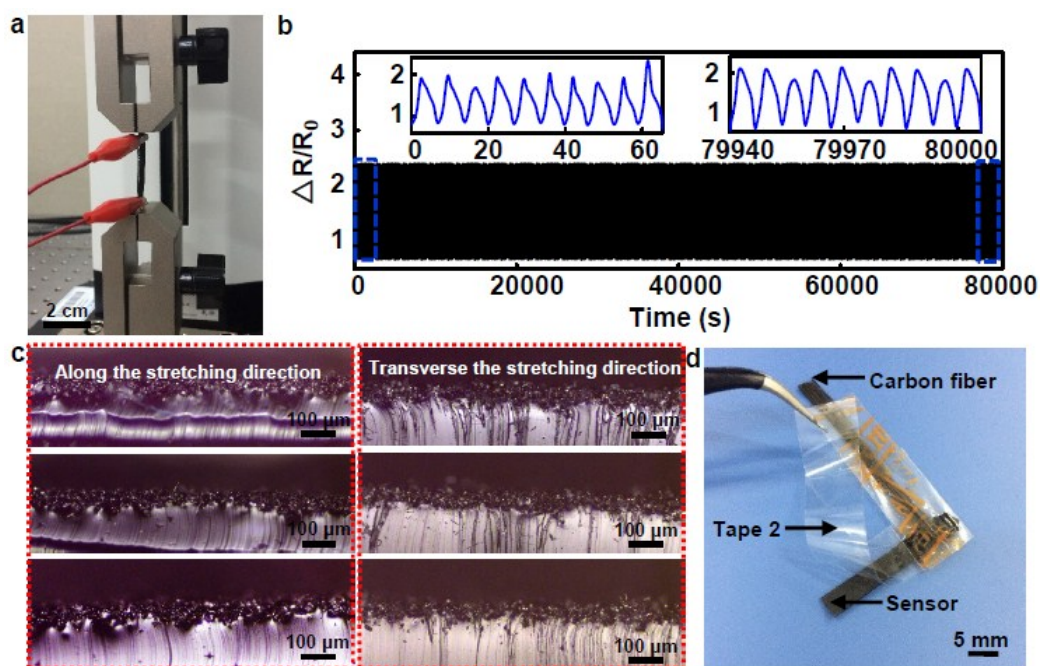


**Figure S9.** (a) A photograph showing the cycling test setup. (b) Relative resistance change of the sensor subjected to more than 10,000 cyclic tension test. (c) Cross-sectional optical images of the sample after the cyclic tension test. (d) A photograph showing the adhesion test for the sample after the cyclic tension test (The carbon fiber was used as the current collector).

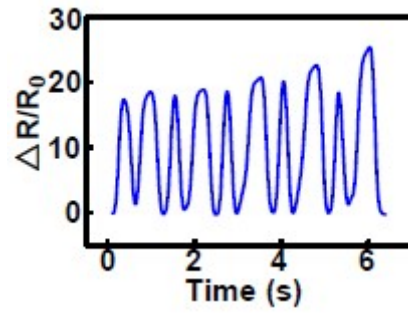


**Figure S10.** Dynamic response of the strain sensor with a density of  $1.07 \text{ mg cm}^{-2}$  to large loading/unloading cycles (10 cycles at strain of 80%).

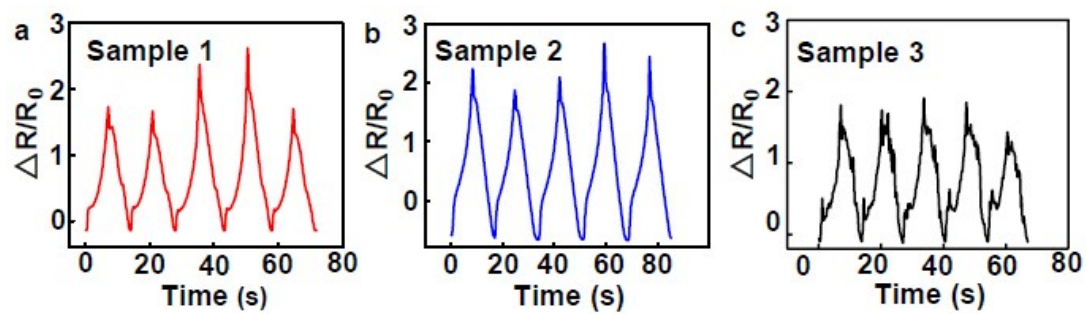


**Figure S11.** The relative resistance changes of the three strain sensors with FCMS density of  $1.07 \text{ mg cm}^{-2}$  in response to stretching-releasing cycles.

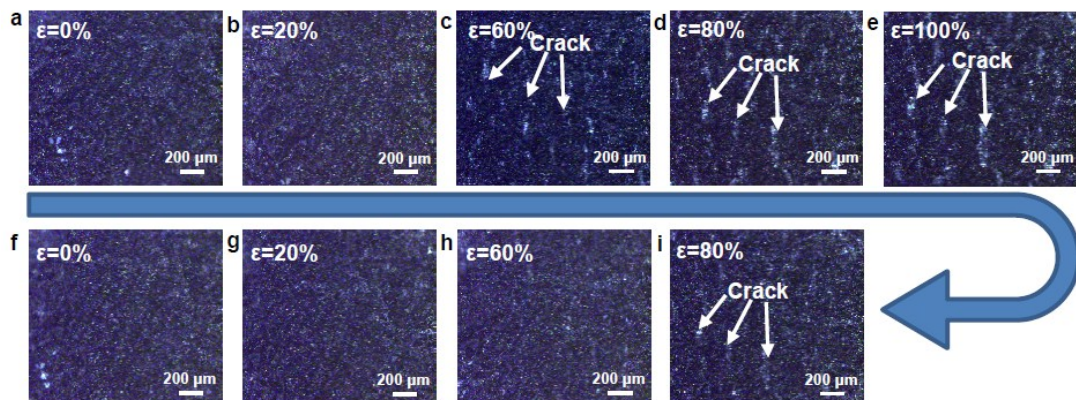


**Figure S12.** In situ tension tests of the FCMS-based strain sensor with a density of 1.07 mg cm<sup>-2</sup>. (a-d) Sequential optical images of the strain sensor under different uniaxial strains.

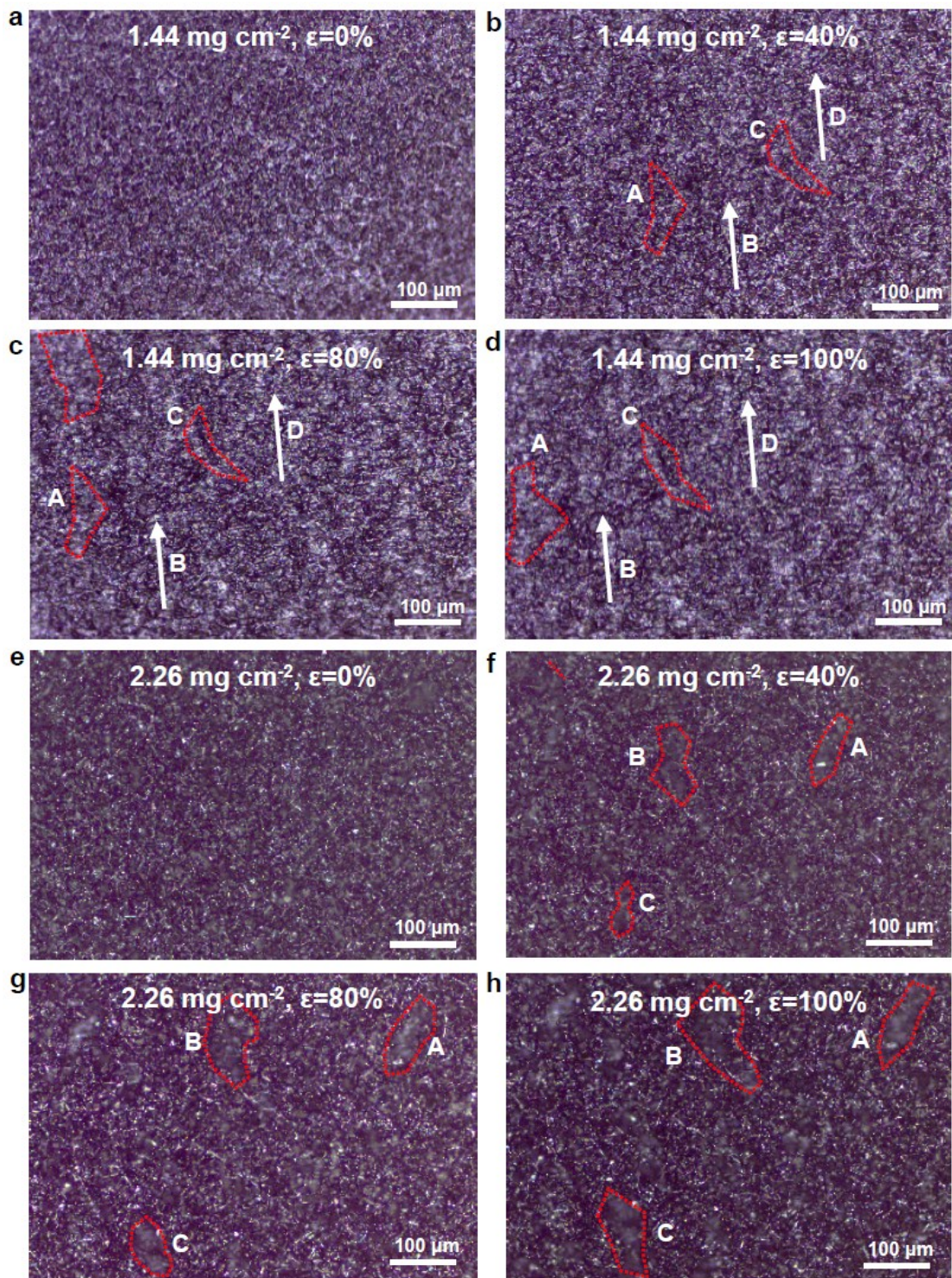


**Figure S13.** (a-d) Sequential optical images of the strain sensor with a density of 1.44 mg cm<sup>-2</sup> under different uniaxial strains. (e-h) Sequential optical images of the strain sensor with a density of 2.26 mg cm<sup>-2</sup> under different uniaxial strains.

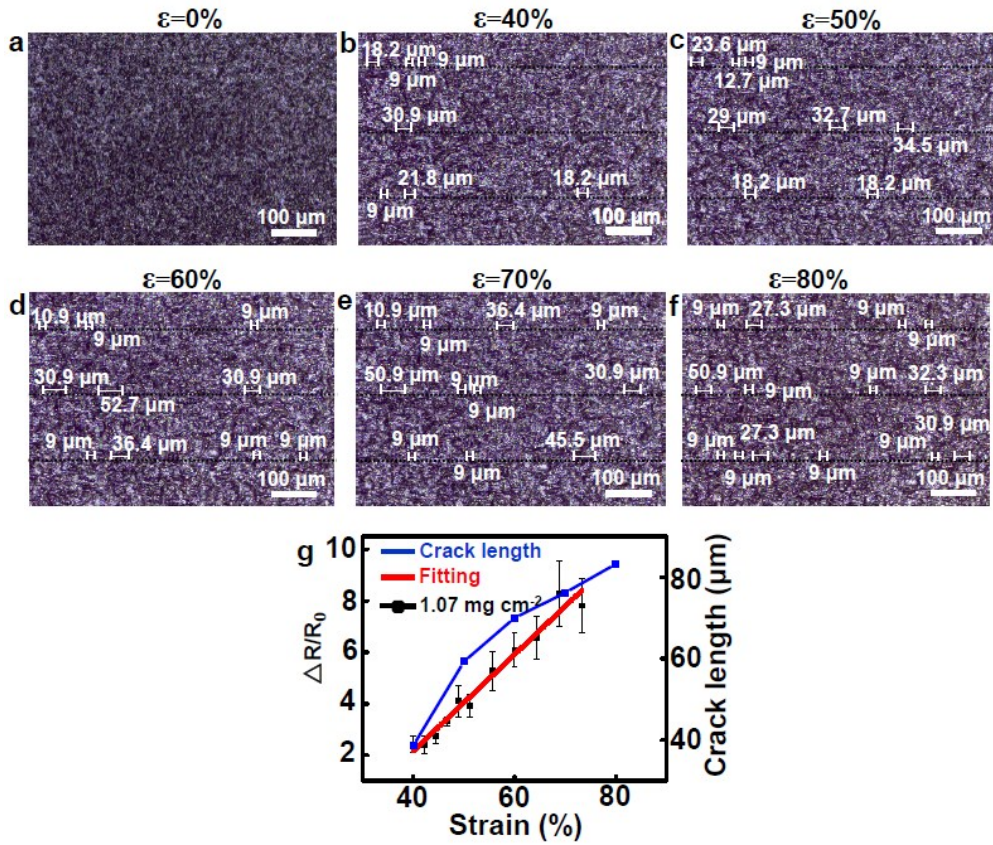


**Figure S14.** (a-f) Sequential optical images of the strain sensor under different uniaxial strains. (g) The relative resistance change and crack length of the sample subjected to different strains.

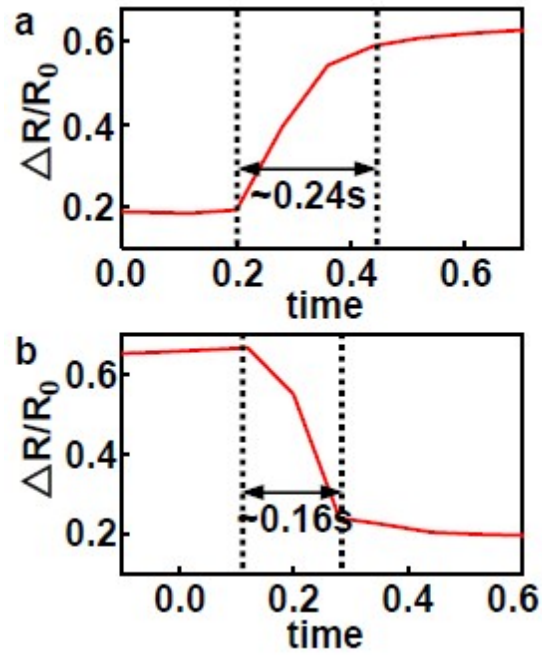


**Figure S15.** The response time of the FCMS-based strain sensor.

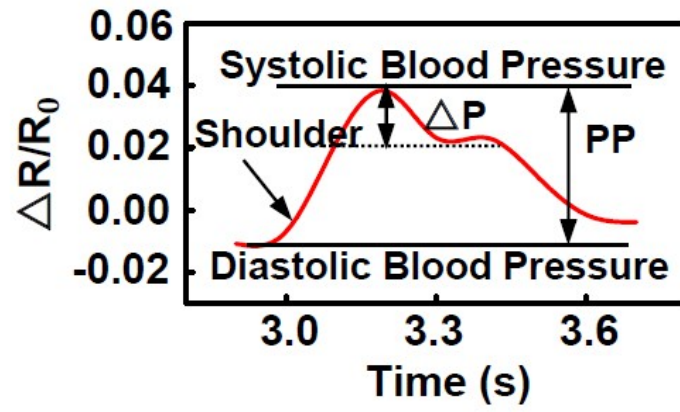


**Figure S16.** The carotid arterial pressure waveform measured by the FCMS-based strain sensor.

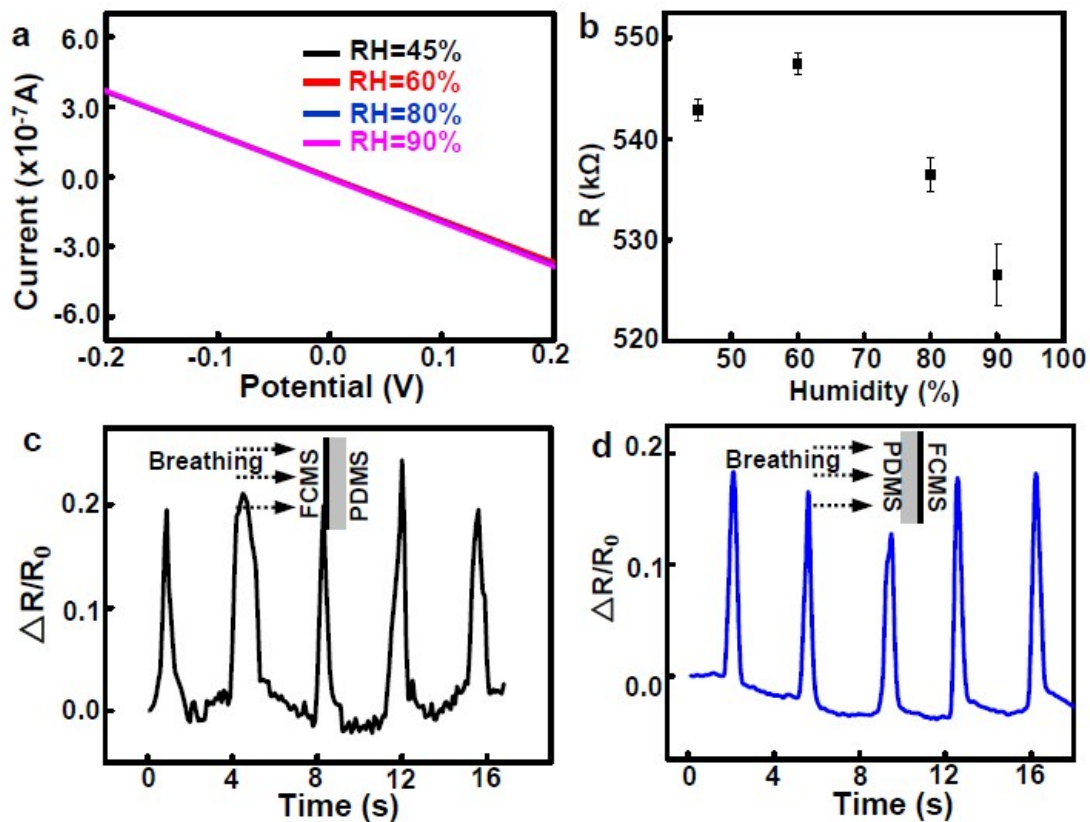


**Figure S17.** (a) Current-voltage curves of the strain sensor at environments with different RHs. (b) The resistance of the sensor at different RHs. (c) and (d) The relative resistance changes of the strain sensor in response to human breathing using two different experimental setups (i.e., Substrate facing to mouth, and FCMS facing to mouth).